JOURNAL OF PROPULSION AND POWER
Vol. 9, No. 4, July–Aug. 1993

# Blade Row Interaction Effects on Compressor Measurements

T. Shang,* A. H. Epstein,† and M. B. Giles‡
*Massachusetts Institute of Technology, Cambridge, Massachusetts 02139*
and
A. K. Sehra§
*Textron Lycoming, Stratford, Connecticut 06497*

**The influence of a downstream stator row on the measurement of compressor rotor performance has been examined using a two-dimensional computational fluid dynamic (CFD) code backed by laser anemometry data on a transonic fan stage. The upstream potential influence of the stator causes unsteady circulation about the rotor blades which is a function of the rotor circumferential position. This, in turn, results in a nonuniform circumferential pattern of time-averaged temperature and pressure in the stationary frame. A relatively fast calculational procedure using a linearized, potential flow approach coupled with an analytical theory relating the temperature and pressure variations to the circulation perturbation is developed and shown to give good agreement with the numerical calculations. The results of a parametric study show that the magnitude of this effect is a strong function of rotor-stator blade row spacing and relative blade counts. The effects range from negligible for large spacings typical of high bypass ratio fans, to several percent of the stage pressure and temperature rise for closely spaced blade rows typical of high compressors. Because the temperature and pressure perturbations are in spatial phase, the net effect on measured rotor efficiency is negligible so long as the pressure and temperature measurements are made in the same location relative to the stators. If they are not, errors of ±1.5% can result. The effects of axial position and stator loading are shown to be relatively small.**

## Introduction

AERODYNAMIC performance measurements are the most basic of turbomachinery tools required for research, design verification, and development. By performance, we refer to measurements of average temperature and pressure made of the machine inflow and outflow, as well as between the blade rows, used to deduce the turbomachine work and efficiency. It has long been recognized that the interpretation of these measurements is far from straightforward.

Because these turbomachine flowfields are spatially nonuniform and highly unsteady, questions concerned with averaging have received considerable attention. These concerns have started at the probe inlet (how do conventional pitot type probes behave in unsteady flowfields[1–3]) and continue through to measurement interpretation (which averaging technique—time, mass, stream thrust, etc.—most closely represents the thermodynamic quantities of interest[4]). Here, we are concerned with questions of spatial uniformity and spatial averaging.

The best agreements between aerodynamic and shaft torque-based efficiency measurements are generally found when the aerodynamic measurements are made far downstream of the turbomachine in a region of uniform flow. In this case, the fluid mechanics of mixing have homogenized the flow, effectively spatially averaging the temperature and pressure (and incurring a mixing loss in the process, of course). Often, such preferred probe placement is not possible. The probes may be embedded within the blade rows and often, to reduce blockage, within the stators themselves. This is especially true in cases in which the rotor performance is required, in multistage machines when individual stage behavior must be measured, and in small machines in which instrumentation placement is extremely constrained by blockage and access problems.

Any stationary intraturbomachine instrumentation placement is dependent on the presumption that the flow is uniform in the pitchwise direction to the degree that it is adequately sampled by relatively few rakes mounted about the circumference. For stator leading-edge-mounted probes in compressors, e.g., the flow is presumed to be completely azimuthally uniform since only one pitchwise position relative to the stators (e.g., the stator leading edge) is sampled. We know that the flow is not uniform in the case of multistage machines in which upstream stators clearly introduce azimuthal variation. Circumferential traversing of probes and rakes solves this problem but is often not done (especially in compressors) due to access, blockage, or cost considerations. The goal of the work described herein was to examine the importance of probe placement to the measurement of aerodynamic performance in high-speed compressors, and then generate guidelines for probe placement and/or data "correction."

The methodology adopted was to employ a multiblade row, unsteady two-dimensional computational fluid mechanics (CFD) calculation as the basic tool, and compare measurements at various locations as calculated by the code with the true mass-averaged performance of the compressor. The basic fidelity of the calculation was assessed by comparison of the CFD results with laser anemometer measurements where available. A linearized potential theory approach was also developed, which is fast and inexpensive enough for routine use in experiment design and data reduction. The following sections describe the calculational procedure, the compressor examined, the code verification, the calculated spatial variation of aerodynamic performance, a discussion of fluid mechanic mechanisms generating the variations, and the implications and recommendations for the accuracy of performance measurements.

Received July 12, 1991; revision received Jan. 5, 1993; accepted for publication Feb. 15, 1993. 

*Graduate Research Assistant, Gas Turbine Laboratory, 31-256.
†Professor, Gas Turbine Laboratory, 31-266. Associate Fellow AIAA.
‡Associate Professor, Gas Turbine Laboratory, 31-264. Member AIAA.
§Manager, Compressor Aerodynamics, Department LSD-10, 550 Main Street.

## Calculational Procedure

The basic tool for this study was a two-dimensional, multiblade row, unsteady, computational fluid mechanics code known as UNSFLO. UNSFLO uses Ni's explicit Lax-Wendroff method to solve the unsteady Euler equations on an unstructured grid of quadrilateral cells. A time-inclined computation plane facilitates the calculation of stages with unequal rotor-stator numbers, greatly reducing the computation time required. For the calculations presented here, approximately 16,000 grid points were used. The computations were done for either one rotor and one stator passage, or two rotor and three stator passages, depending on the relative blade row count. The time tilting then serves to adjust the calculation to the desired blade row pitch ratio. More details on the solution method can be found in Refs. 5 and 6.

Approximately 10,000 iterations were required for an initial steady-state solution with an approximately equal number required to achieve unsteady periodicity (this was approximately 30 blade passing periods). A typical solution time was approximately 10 h on a three-processor Alliant FX/8 computer, 6 h on a Stellar, or 90 h on a DEC $\mu$VAX-III (all three machines were used at different times).

The work described herein uses an inviscid version of the code. A specific advantage of UNSFLO for this investigation is that it permits essentially arbitrary rotor-stator pitches (blade counts) while incurring little computational overhead. This greatly facilitates parametric examination of the importance of stage design parameters on measurement accuracy.

## Compressor Description

The compressor chosen for this study is a 1.68 pressure ratio, low-aspect ratio, single-stage transonic fan stage designed at the NASA Lewis Research Center in the mid 1970s.[7] Known as stage 67, this 0.5-m-diam machine was selected primarily because of the large amount of experimental data—including laser anemometry[8,9] and time-resolved intrastage flow measurements[10]—which are in the public domain. Also, there is a considerable number of two-dimensional, three-dimensional, inviscid, and viscous calculations published on this geometry.[11,12] The flow path is shown in Fig. 1. Calculations were done only for the two-dimensional stream-surface indicated, which is slightly outboard of the sonic radius. This position was selected because of the availability of both laser anemometer and high-response probe data at that location as well as a detailed, unsteady two-dimensional viscous solution.[12]

## Verification of CFD Calculation

Although UNSFLO had been shown to give quite good results with turbines, it had not been previously used for high-speed compressors. Therefore, it was thought important to establish the fidelity of the calculation by comparison with data. Also, the influence of the inviscid flow assumption had to be assessed. Table 1 compares the calculated and measured values of specific flow (mass flow per unit area), and the stage pressure and temperature ratio at the stage exit along the selected streamline at the design point conditions. These are quite close for an inviscid calculation. At this condition, there is a small discrepancy between the axial location of the calculated and measured (by laser anemometry[8]) shock wave positions shown in Fig. 2. This can be explained by a small difference in rotor blade incidence angle and the absence of boundary-layer blockage in a design with small choke margin.

The circumferential variation in the time-averaged total temperature, as calculated with the Euler turbine equation from the circumferential velocity change at an axial station between the rotor and stator, is shown in Fig. 3 for both the laser anemometer data and the CFD calculation. Although the absolute levels differ by a small amount, the level of circumferential variation in temperature is quite well predicted. The experimental and predicted pitchwise variation in axial velocity perturbation also agree well (Fig. 4).

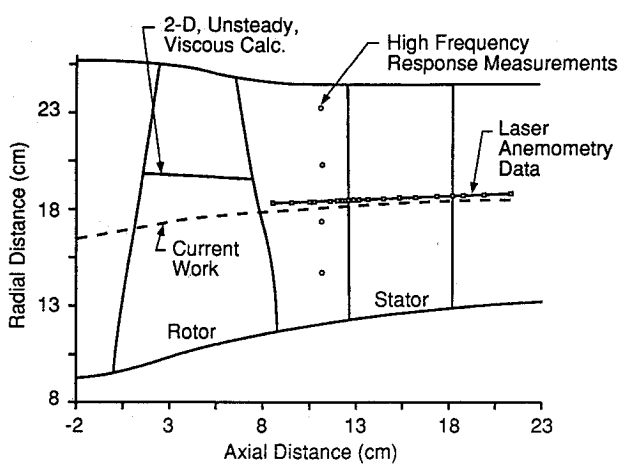


**Fig. 1 Flow path of NASA LeRC stage 67 showing streamline used in this study.**

**Table 1 Comparison of calculated and measured performance along a two-dimensional streamtube near midspan**

| | CFD | Measured |
|---|---|---|
| Specific mass flow, $\rho U$ | 280.1 | 276.8 |
| $P_{t3}/P_{t0}$ | 1.609 | 1.634 |
| $T_{t3}/T_{t0}$ | 1.153 | 1.160 |

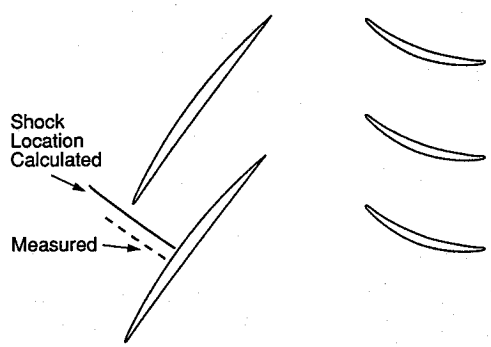


**Fig. 2 Comparison of measured and calculated shock positions.**

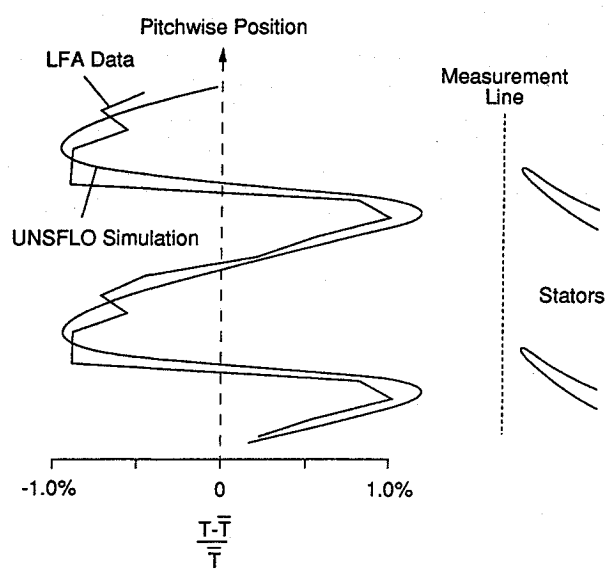


**Fig. 3 Comparison of measured and calculated time-averaged temperature estimated with Euler's turbine equation from the tangential velocity, as a function of pitchwise location. $T$ is the local temperature, $\bar{T}$ the pitchwise-averaged temperature.**

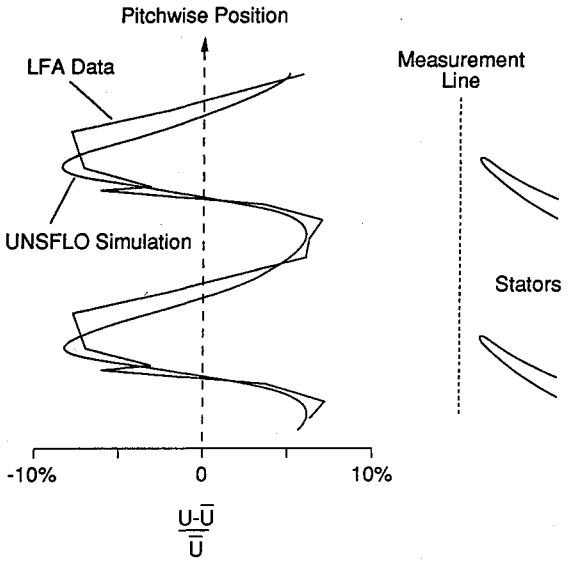


**Fig. 4 As in Fig. 3, but comparison of the time-averaged axial velocity distribution: $U$ is the local axial velocity; $\bar{U}$ the pitchwise-averaged velocity.**

We conclude from comparisons, including those above, that the inviscid CFD calculation is capturing the essential features of the flowfield, giving an adequate picture of the spatial distribution of the compressor flow.

## Calculational Results

The Euler temperature measurements and calculations of Fig. 3 show a significant variation in the flowfield temperature with pitchwise position, about ±1% (6 K). Before looking in more detail at probe placement effects, let us try to understand why the flowfield in the compressor behaves in this manner—what causes flow variations on the order of the stator spacing? An obvious answer is the upstream influence of the potential field of the stator on the rotor aerodynamics. Indeed, this can be seen in the variation of rotor blade circulation and lift with pitchwise position (Fig. 5). The change in circulation results in the shedding of vorticity downstream of the rotor (Fig. 6). In addition, the change in lift and back pressure moves the passage shock wave, varying its strength and thus the entropy it produces. This is the only explicit source of loss in this inviscid calculation. Since the work done by the rotor blade varies with position, the temperature and pressure fields will vary as well.

## Vortex Sheet Analysis of the Time-Averaged Spatial Flow Variation

Given the variation in rotor blade circulation induced by the potential field of the downstream stators, we can calculate the spatial variation in the time-averaged flowfield analytically as well as numerically. Horlock[13] calculated the stagnation pressure variation due to the circulation change for an incompressible flow using a continuous vortex sheet model, assuming the distribution to be sinusoidal (i.e., considering only the first spatial harmonic). Here, we attack the problem somewhat differently, permitting arbitrary spatial variation and generalizing the analysis to enthalpy variation so that compressible flow may be analyzed.

In the absolute, stator frame of reference, the flow can be modeled as a sequence of propagating vortex sheets passing through an otherwise irrotational flowfield. Since the unsteady circulation around the rotor blades is phase-locked to the stator motion relative to the rotors, in the absolute frame the flowfield is periodic in time, with the period being equal to the rotor blade passing period. Thus, at a fixed point in the absolute frame, the vortex sheets which pass by always

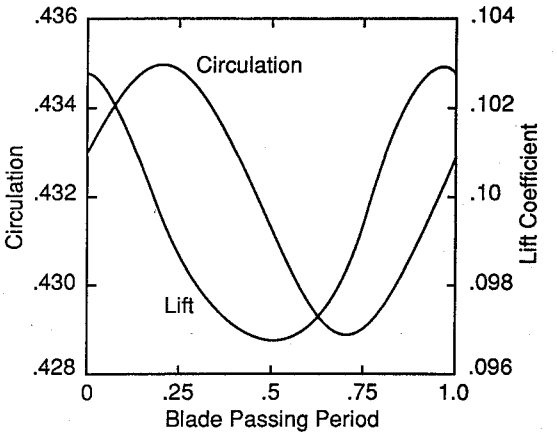


**Fig. 5 Time variation of rotor blade circulation and lift as a function of blade passing period (time required to traverse one stator pitch).**

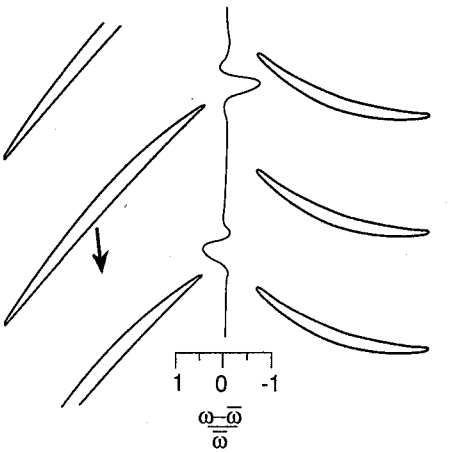


**Fig. 6 Pitchwise vorticity distribution at one instant in time illustrating the magnitude of the shed vorticity perturbation $\omega$ compared to the time-averaged vorticity $\bar{\omega}$.**

have the same strength. It is this fact which causes the time-averaged stagnation enthalpy to be spatially nonuniform.

The starting point for the analysis is Crocco's theorem in the absolute (stator) frame of reference

$$T\nabla S + \boldsymbol{u} \times \boldsymbol{\omega} = \nabla H_0 + \frac{\partial \boldsymbol{u}}{\partial t} \tag{1}$$

with the temperature $T$, the entropy $S$, the velocity vector $\boldsymbol{u}$, the vorticity $\boldsymbol{\omega}$, and the stagnation enthalpy $H_0$.

Assuming that the flow is isentropic and irrotational, *except* for the passing unsteady vortex sheets shed by the rotors due to their varying circulation, time-averaging gives

$$\nabla \overline{H_0} = \overline{\boldsymbol{u} \times \boldsymbol{\omega}} \tag{2}$$

where the sole contribution to the time average $\overline{\boldsymbol{u} \times \boldsymbol{\omega}}$ comes from the passing vortex sheets.

Defining $\boldsymbol{u}_\omega(x, y)$ to be the local velocity $\boldsymbol{u}(x, y, t)$ at the time $t$ at which the vortex sheet passes the point $(x, y)$, $y$ being the tangential direction, it follows that

$$\boldsymbol{u}_\omega \cdot \nabla \overline{H_0} = 0 \tag{3}$$

and therefore, $\overline{H_0}$ is constant along pathlines generated by vortex sheet elements.

Given this result for the "convection" of $\overline{H_0}$, it is now sufficient to find the variation of $\overline{H_0}$ in the circumferential $y$ direction, at the $x$ location corresponding to the rotor's trailing edge.

With a suitable choice of origin, the position of the trailing edge of one particular rotor blade is given by $(x, y) = (0, V_w t)$, where $V_w$ is the rotor wheel speed. Near the trailing edge, the vorticity distribution is given by a delta function in a coordinate system which is rotated to be normal to the vortex sheet:

$$\omega(x, y, t) = -\gamma\delta[(y + V_w t)\cos\beta - x\sin\beta] \quad (4)$$

$\beta$ is the rotor-relative flow angle at the trailing edge, and $\gamma$ is the strength of the vortex sheet shed at the trailing edge of the rotor which varies as the rotor moves, and so is a function of the position of the trailing edge. Kelvin's theorem (which is valid for an isentropic compressible fluid) gives the following relationship between $\gamma(y)$ and $\Gamma(y)$, the circulation around the rotor which is also a function of $y$, the position of the trailing edge:

$$U\gamma = -\frac{d\Gamma}{dt} = V_w \frac{d\Gamma}{dy} \quad (5)$$

In the above equation, $U$ is the magnitude of the rotor-relative velocity at the trailing edge, averaged over the two sides of the trailing edge. With these pieces, and defining $\tau$ to be the blade passing period, it is now possible to calculate the variation of $\overline{H_0}$ in the $y$ direction:

$$\begin{aligned}\frac{\partial\overline{H_0}}{\partial y} &= -\overline{u\omega}\cdot\cos\beta \\ &= -U\cos\beta\frac{1}{\tau}\int_0^\tau \omega\, dt \\ &= \frac{U\gamma}{\tau V_w} \\ &= \frac{1}{\tau}\frac{d\Gamma}{dy}\end{aligned} \quad (6)$$

Integrating this equation produces the final, simple relationship between the perturbation in the time-averaged stagnation enthalpy $\overline{H_0'}$ and the perturbation in the circulation $\Gamma'$:

$$\overline{H_0'} = \frac{\Gamma'}{\tau} \quad (7)$$

This analysis, of course, does not tell us what the circulation perturbation is; a suitable linearized potential flow method is presented in the next section.

We can, however, take the circulation perturbation from the numerical analysis (Fig. 5), and use that to predict the spatial variation in stagnation enthalpy. This is compared to the numerically calculated variation and to that predicted using Horlock's method[13] in Fig. 7. The close agreement among the three is primarily a consistency check between the analytical and numerical methods, lending credence to both. It also shows that, at least for this geometry, the spatial variation in circulation is essentially sinusoidal and that those phenomena modeled numerically but not analytically—e.g., shock wave effects—are not important here.

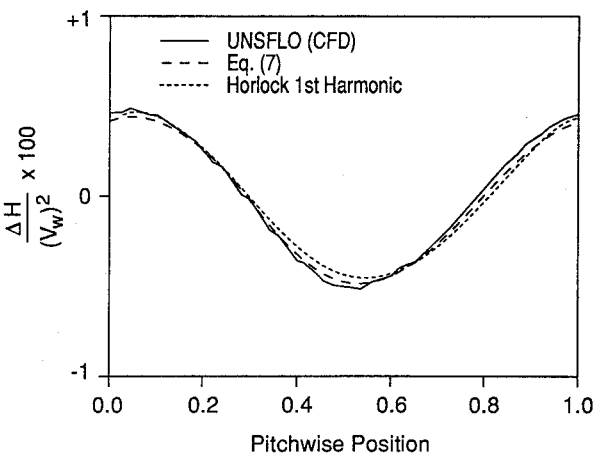


**Fig. 7 Pitchwise enthalpy distribution as calculated by the CFD code UNSFLO, Eq. (7), and using Horlock's methods.[13]**

## Linearized, Potential Flow Approach

Now that it has been established that the spatial variations in time-averaged enthalpy are principally due to inviscid, potential flow effects, alternate calculational approaches are attractive. Although UNSFLO gives accurate results and is relatively fast for a full unsteady, multiblade row code, it can be expensive to run on a routine basis. We therefore explored an alternate approach which results in a considerable reduction in computer time.

Using Eq. (7), the time-averaged enthalpy variation can be found given the temporal perturbation of rotor circulation. This circulation perturbation results from the spatial perturbation in the pressure upstream of the stator row, i.e., the upstream potential flow influence. Thus, the spatial variation in enthalpy can be calculated in three relatively fast (and simple) steps. First, calculate the potential field upstream of an isolated stator row of the given geometry. This can be readily done in a number of ways, for example, panel methods codes are quick and widely available. Here, we used a single blade row, steady version of UNSFLO for expediency. Second, using the circumferential potential variation estimated in step one, calculate the time variation in rotor circulation. Since the phenomena of interest are inviscid, a linearized, unsteady, flat plate program should give adequate results. Here, we used the program LINSUB written by Whitehead[14] based on theory by Smith.[15] LINSUB outputs the vortex sheet strength shed by the rotor which was then converted to circulation using Kelvin's theorem [Eq. (5)]. The third step is to use Eq. (7) to calculate the enthalpy variation given the circulation perturbation calculated in step 2.

A comparison of the results of this technique with those from the multiblade row version of UNSFLO is given in Table 2. The agreement in maximum amplitude of the enthalpy perturbation predicted by the two methods is quite good. The relative circumferential phase of the perturbations differs by as much as 16% of the stator pitch. [The UNSFLO results agree with the phase measured by the laser anemometer only to about 5% (Figs. 3 and 4).] It is important to note here that since the maximum value of the enthalpy perturbation is al-

**Table 2 Comparison of circumferential enthalpy variation calculated with two different methods**

| | Case 1 | | Case 2 | | Case 3 | |
|---|---|---|---|---|---|---|
| Rotor-stator gap (% of rotor chord) | 10% | | 20% | | 20% | |
| Rotor-stator pitch ratio | 1.45 | | 1.45 | | 0.94 | |
| | Mag. | Phase | Mag. | Phase | Mag. | Phase |
| Max normalized enthalpy variation ($\rho\tilde{H}/\tilde{P}_{TE}$) amplitude and phase[a] from | | | | | | |
| a) UNSFLO (Euler, nonlinear) | 0.175 | 15 deg | 0.160 | 37 deg | 0.264 | 57 deg |
| b) LINSUB (Linearized potential) | 0.170 | 35 deg | 0.158 | 42 deg | 0.220 | 27 deg |

[a]Phase of peak relative to stator leading edge.

ways quite small (less than 2% of the enthalpy rise across the rotor), the differences between the two methods in the example presented herein may be considered negligible.

The linearized potential flow approach offers an alternate method for estimating the spatial variations in rotor enthalpy. It requires very little computer time (less than 1% of UNSFLO's) and is therefore well-suited for use in experiment design or data reduction.

## Parametric Examination of the Influence of Design Variables

If the pitchwise flowfield variation is primarily due to the potential field of the stators, we would expect that the magnitude of this effect to vary with stage design parameters—in particular, with the axial distance between the rotor and stator (the gap) and the relative spacing between adjacent stator blades compared to the spacing between rotor blades (the pitch ratio). The rotor-stator gap should be important since the potential influence of the stators should die out exponentially upstream of the stators. Thus, increasing the gap should decrease the pitchwise flowfield variations. Similarly, increasing the pitch ratio (the number of stator blades relative to the number of rotor blades) should decrease the pitchwise flow variation since in the limit of an infinite number of stators, the time-averaged pitchwise flowfield must be uniform.

We infer from the above that it is important to parametrically examine the influence of these effects, especially since, depending upon the application, there are very large variations in rotor-stator gap and pitch ratios. Gaps can vary from as low as 10% of rotor chord in high compressors to 400% in high-bypass ratio fans. Also, the gaps are, in general, not fixed but can vary with radius due to blade sweep. Similarly, pitch ratios can vary from 2 to 0.1 (a few large struts about the circumference). The stage studied has a design gap of 0.78 (axial distance between rotor trailing edge and the stator leading edge divided by the rotor axial chord) and a pitch ratio of 1.45 (rotor pitch divided by stator pitch). The relatively large gap had been selected to facilitate detailed intrastage measurements. Because the UNSFLO CFD code readily accepts essentially arbitrary pitch ratios, it was straightforward to parametrically vary the gap and pitch ratio of the calculations (the stator pitch was varied, the rotor pitch held constant—essentially stator blades were added or deleted).

The calculated pitchwise variations in the time-averaged rotor temperature and pressure ratio for a gap of 0.2 and pitch ratio of 1.45 are shown in Fig. 8 for measurement simulated at two axial stations upstream of the stator leading edge, 15 and 20% of the stator axial chord. There are several important observations to make here. The first is that the pitchwise variation in flow quantities is quite substantial, so these are not negligible effects. The second is that the pitchwise distribution of temperature and pressure are more sensitive to the axial measurement location than is the magnitude of the variation. The third observation is that the pressure and temperature variations are in phase with each other and of similar

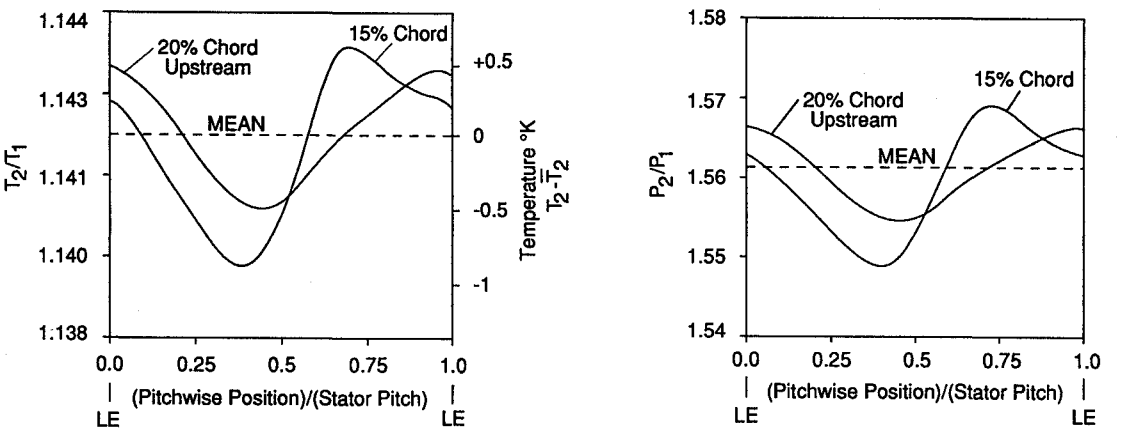


**Fig. 8 Pitchwise distribution of time-averaged stage temperature and pressure ratio at two axial locations (as percentage of stator axial chord). The rotor-stator gap is 0.2 and the rotor-stator pitch ratio is 1.45.**

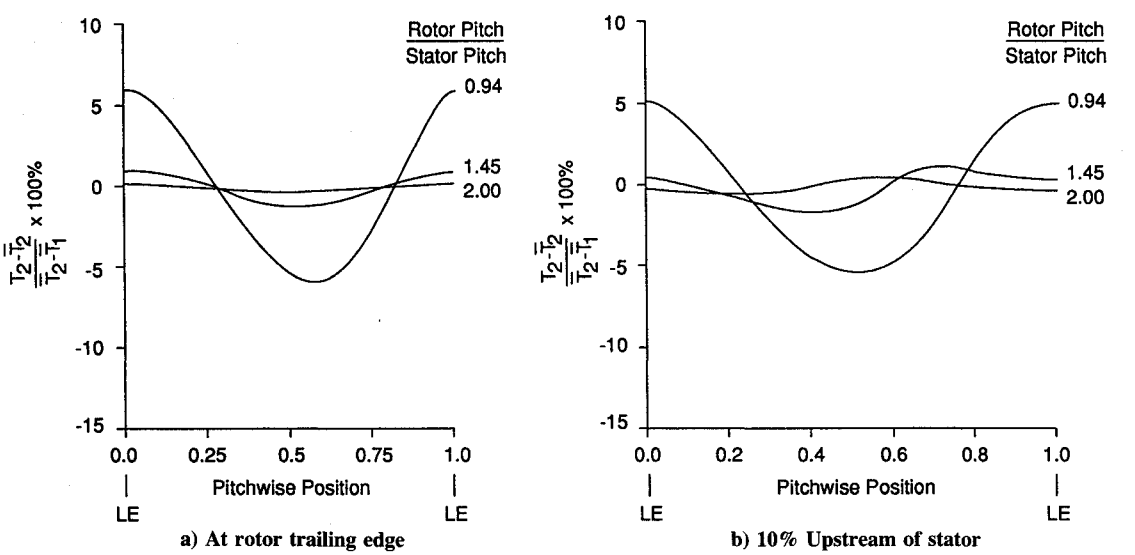


**Fig. 9 Effect of rotor-stator pitch ratio (number of stators/number of rotors) on the normalized, time-averaged temperature rise as would be measured at different pitchwise positions.**

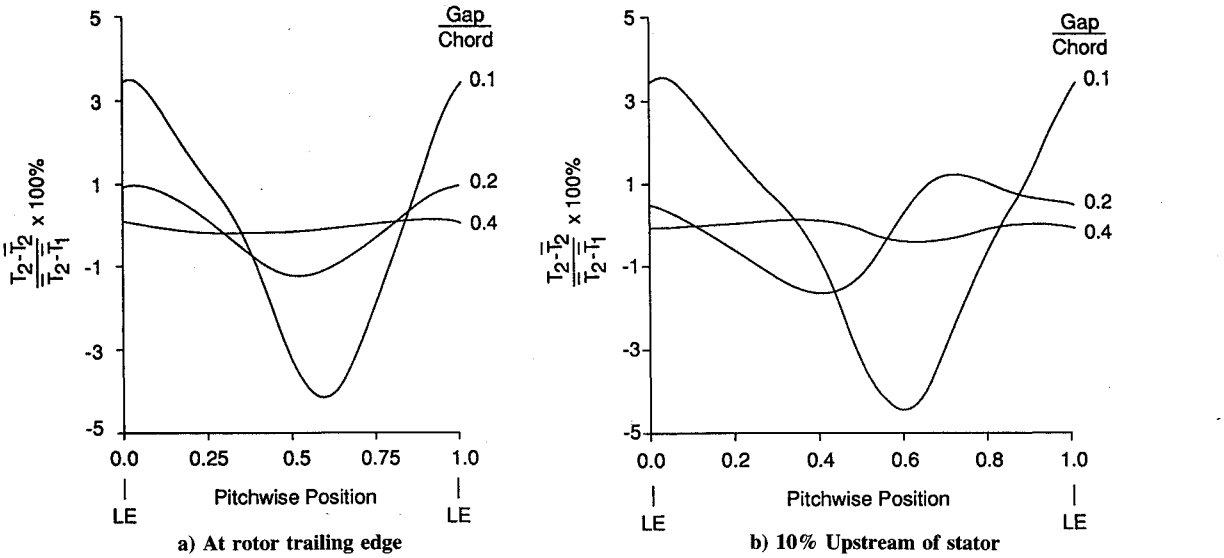


**Fig. 10 Effects of rotor-stator spacing (gap) on the normalized, time-averaged rotor temperature rise as would be measured at different pitchwise positions.**

magnitude. For this reason, we will only present the results for temperature ratio from here on. Both time and mass averages were calculated, but differed by less than 0.002% for these flows, so that only time averages are presented.

The pitchwise variation in the time-averaged total temperature between the rotor and stator is shown in Fig. 9 as a function of rotor-stator pitch ratio for a fixed gap of 0.2 for two axial measurement stations immediately behind the rotor and 10% of stator chord upstream of the stator leading edge. The temperature is plotted as the local deviation from the pitchwise mean (the time-averaged local temperature, $T_2$, minus the pitchwise average of the time-averaged total temperature, $\bar{T}_2$) normalized by the mean rotor temperature rise ($\bar{T}_2$ minus the average rotor inlet total temperature, $\bar{T}_1$). Note that the magnitude of the pitchwise temperature variation changes from quite small at large pitch ratios (2) to quite large at pitch ratios approaching 1. The difference in distance between the rotor and stator in the three cases implies a difference in convection times from the rotor trailing edge to the stators, thus the relative phase shift seen in the near stator leading-edge plots. The variation with rotor-stator gap for the same two axial stations is shown in Fig. 10 for a fixed pitch ratio of 1.45. Note here that, at the gaps typical of fans (0.75–4), the effects are small; but at the closer spacing typical to compressors, the spatial variation becomes significant.

The above plots reflect the pitchwise nonuniformity of the time-averaged flowfield. They also illustrate that the flow is nonuniform in the axial direction as well. While the variation with pitchwise position is larger than that for axial position, the axial variation is not negligible.

## Effects of Measured Efficiency

A primary measure of compressor performance is adiabatic efficiency, which can be calculated from the measured total temperature and pressure. The efficiency calculated from the time-averaged temperature and pressure at each pitchwise location in Fig. 8 is plotted in Fig. 11 as the efficiency perturbation—the local efficiency $\eta$ minus the pitchwise mean $\bar{\eta}$. Here, we see that the variation of efficiency with pitchwise location is very small, although the variations of pressure and temperature are not. The reason for this is that the pitchwise flow variations result predominantly from the variation in rotor blade lift and work as the rotor blades pass through the potential field of the stator blades. This variation in work is performed at essentially constant efficiency (at least in this inviscid calculation) so that the pitchwise variation in temperature and pressure are in phase, as can be seen in Fig. 8.

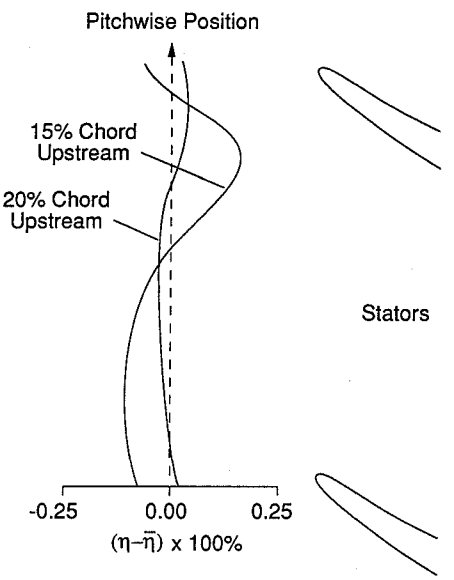


**Fig. 11 Adiabatic efficiency deviation from the pitchwise mean for the flow in Fig. 8 at two axial stations upstream of the stator leading edge.**

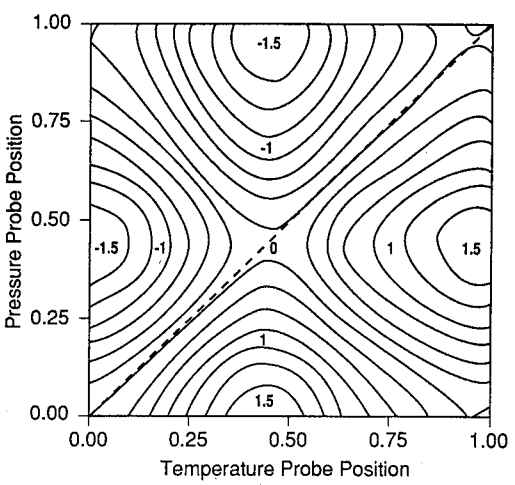


**Fig. 12 Error in efficiency (deviation from the average efficiency) as a function of the locations of the temperature and pressure probes relative to each other and the stators. ----- is the line of similar placement.**

It is very important to note that small efficiency variations seen in Fig. 11 are based on the presumption that the pressure and temperature are measured in exactly the same pitchwise location. This is not necessarily the case in all measurement programs. The result of arbitrary pitchwise location of the temperature and pressure probes relative to each other and the stator leading edges at one axial location is shown in Fig. 12 as contours of local adiabatic efficiency error (the local value minus the average). The variation for the worst case (one probe in midpassage, the other at the stator leading edge) is 3%, a significant error. We conclude from this that it is extremely important to locate pressure and temperature instrumentation at the same pitchwise locations relative to the stator blades to avoid this type of sampling errors.

## Measurements near the Stator Leading-Edge Plane

Instrumentation on multistage compressors is most commonly done by cantilevering probes from the stator leading edge, in order to minimize blockage. Fortunately, this will also minimize the sampling errors in efficiency measurement by ensuring that the probes are placed at the same relative pitchwise location, as mentioned above.

We wished to examine whether small changes in axial probe position near the stator leading-edge plane would influence accuracy (in other words, does the length of the pitot tube cantilever matter). In this inviscid calculation, the leading-edge flows are not resolved in sufficient detail to permit an accurate assessment in that region. Therefore, the flow near midpassage was examined. Figure 13 shows the deviation in measured efficiency for small changes in the probe axial location. The effects are essentially negligible.

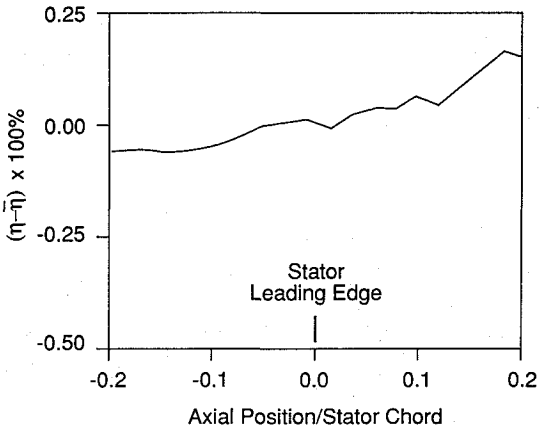


**Fig. 13 Variation in apparent efficiency measurement with probe axial position near stator midpassage.**

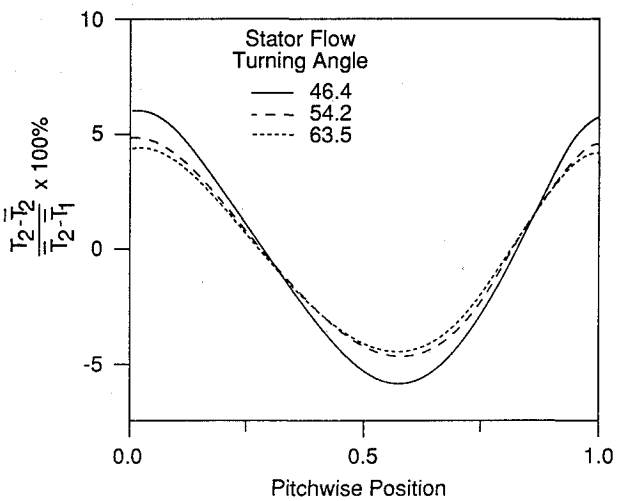


**Fig. 14 Influence of stator loading on rotor outflow pitchwise temperature distribution.**

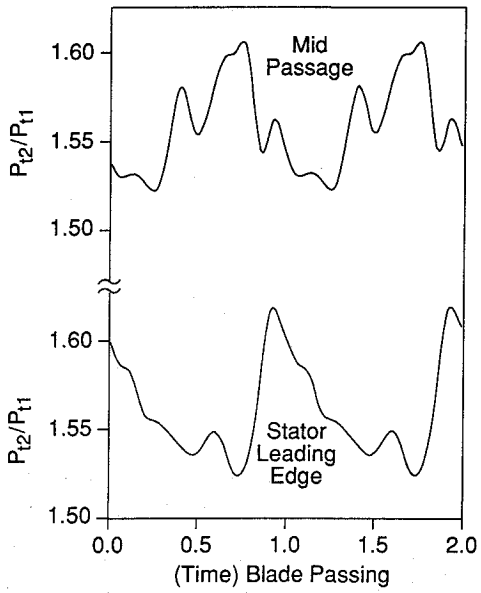


**Fig. 15 Instantaneous total pressure as would be measured at two pitchwise locations at midrotor-stator gap.**

## Influence of Stator Loading

The influence of stator loading on the blade row interactions was examined by generating a family of similar airfoils with differing camber. The results are illustrated in Fig. 14, which shows a relatively small influence on rotor exit temperature distribution for a ±8 deg change in stator turning.

## Time Unsteady Flow

So far, we have examined only the time-averaged flowfield. The time-resolved flow is, of course, influenced by the blade row interaction as well. The spatial distribution of the time average is a reflection of the variation of the time-resolved rotor exit flowfield with instantaneous pitchwise position. This is illustrated in Fig. 15, which shows the instantaneous pressure ratio at two pitchwise positions upstream at the same axial station in the rotor stator gap. Note that the waveform shape changes as well as the mean level. This may introduce an error in pitot type probes, as was pointed out by Weyer.[1]

## Conclusions

The work reported herein has concentrated on examining the influence of rotor-stator interactions on the measurement of compressor rotor performance. The results can be summarized as follows:

1) The upstream potential field of the stators results in unsteady lift on the upstream rotor blade.

2) The unsteady rotor lift results in circumferential or pitchwise nonuniformity of the rotor exit time-averaged flowfield.

3) The magnitude of the pitchwise nonuniformity is strongly dependent on the rotor-stator spacing and the relative number of rotor and stator blades.

4) At blade row spacings typical of high-bypass ratio turbofans, the nonuniformity is negligible.

5) At blade row spacings typical of compressors, the flow nonuniformity can be substantial, ±2–3% of the stage average temperature or pressure rise (about 1.5°C for the stage studied).

6) Although the temperature and pressure nonuniformity is large, the adiabatic efficiency is nearly uniform since the temperature and pressure variations are in phase.

7) Stator leading-edge temperature and pressure instrumentation will, therefore, read about 1% high, but the re-

sultant efficiency will be within 0.2% of the true pitchwise average.

8) Placing temperature and pressure instrumentation at different relative circumferential positions can result in large efficiency errors, ±1.5% for the stage studied.

9) A linearized potential flow approach and a multiblade row, time-accurate Euler solution give similar results when used to calculate these variations.

It is important to note that the measurement errors which can be introduced by nonuniform circumferential rotor outflow must be added to any errors introduced by the unsteady response of the instrumentation,[1] which we expect to be somewhat larger in the case of well-designed conventional installations.

Overall, the results presented herein indicate that the time-averaged rotor outflow is not circumferentially uniform. The analytical estimates that nonuniformity presents are in good quantitative agreement with the measurements available. The conclusion is that care must be exercised in the planning and reduction of data from measurements of closely coupled high-performance turbomachinery.

## Appendix: Using a Linearized Flat Plate Cascade Theory to Estimate Measurement Error

Until now, UNSFLO has been the major tool for this investigation. Although UNSFLO proved to be an accurate and efficient CFD code compared to others, it is still relatively expensive in CPU time. Furthermore, since the only quantity we need is the unsteady rotor blade loading (hence, the circumferential total enthalpy variation), it is not necessary to calculate the entire flowfield. An alternative approach is to use the linearized flat plat cascade theory by Smith.[15] This approach also provides physical insight into this phenomenon.

The linearized theory assumes that the time-averaged two-dimensional subsonic flow is uniform in all directions. The cascade consists of flat plates of negligible thickness at zero incidence angle, therefore, the averaged loading on the blade is zero. All flow perturbations from the uniform flowfield are assumed to be small enough so that the flow equations may be linearized and the principle of superposition applied. The unsteady load (circulation) of the cascade due to an external perturbation is then analyzed. In our application, the external perturbation is the potential pressure wave from the downstream stator blade row. The flow is assumed to be isentropic and inviscid.

As pointed out in earlier sections, blade row interaction is primarily an inviscid phenomenon. The shed vortex sheet analysis shows that the assumption of isentropic flow is reasonable in this context. The flow perturbation between the blade row is very small, amounting to less than 10% in velocity variation (Fig. 4). Considering the axial decay, the perturbation close to the rotor would be even smaller. Since the rotor blade camber is fairly flat and most of the unsteady loading is concentated on the rear part of the blade, a flat plate cascade with stagger angle equal to the exit flow angle is an accurate assumption in this case. Figure A1 shows this rotor configuration. The mean flow quantities are taken as the circumferential average of the rotor exit flow.

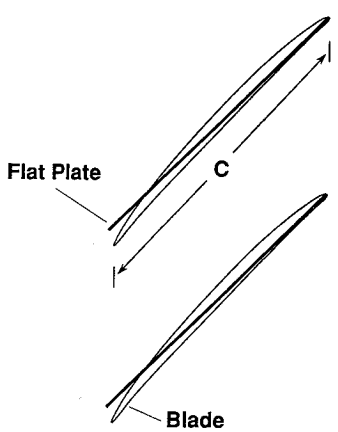


**Fig. A1 Rotor cascade geometry: airfoil and the flat plate approximation.**

A basic driver of rotor unsteady loading is the potential disturbance from the downstream stator blades. If we use the true chord of the blade $C$, averaged density $\rho$, wheel speed $V_w$, and relative velocity $W$ at the rotor exit as the normalizing quantities, the unsteady component of pressure, in the frame relative to the rotor, would be

$$p' = \bar{p} \exp(i\alpha x + \beta y - i\omega t) \tag{A1}$$

where

$p', \bar{p}$ = pressure perturbation and complex magnitude
$x, y, t$ = normalized axial and circumferential coordinate and time
$\beta$ = the $y$ wave number, $\beta = 2\pi(C/S_s)$
$\omega$ = reduced frequency, $\omega = \beta[(V_w)/W]$

The axial wave number $\alpha$ will be determined as the following:

$$\alpha = \frac{1}{\sqrt{1 - M^2 \cos^2\theta}} (M^2 \cos^2\theta(\beta \sin\theta - \omega) - i\sqrt{\Omega^2}) \tag{A2}$$

while

$$\Omega^2 = (1 - M^2)\beta^2 + 2M^2\beta\omega \sin\theta - M^2\omega^2 \tag{A3}$$

Since $\alpha$ has a negative imaginary part, the pressure is exponentially decaying upstream.

The linearized theory predicts that the unsteady loading (circulation) is linearly proportional to the perturbation around the blade. If we assume the unsteady circulation takes the form of

$$\Gamma' = \bar{\Gamma} e^{-i\omega t} \tag{A4}$$

then the nondimensional quantity $\rho W\bar{\Gamma}/C\bar{P}_{TE}$ would be a constant. Here $\bar{P}_{TE}$ is the complex pressure magnitude at the rotor trailing-edge position, generated by the relatively moving stator blade as if the rotor is removed. From the section of shed vortex sheet analysis, we know that

$$H' = (\Gamma'/\tau)$$

If we assume $H'$ in the complex form

$$H' = \bar{H} e^{i\beta y}$$

then the nondimensional quantity for the stagnation enthalpy variation would be $\rho\bar{H}/\bar{P}_{TE}$.

A computer program implementing the linearized flat plat cascade theory, called LINSUB, was written by Whitehead

**Table A1 LINSUB Required input**

| | |
|---|---|
| $S_r/C$ | Cascade solidity<br>$S_r$: Rotor pitch<br>$C$: Rotor chord |
| $\theta$ | Rotor blade stagger angle (also mean flow angle) |
| $M$ | Flow Mach number |
| $\beta$ | Circumferential wave number<br>$\beta = 2\pi\ C/S_s$<br>$S_s$: Stator pitch |
| $\omega$ | Reduced frequency<br>$\omega \equiv \beta(V_w)/W$<br>$W$: Relative flow speed |

**Table A2 Flow parameters and results: UNSFLO and LINSUB**

| Flow parameters | Case 1 | | Case 2 | | Case 3 | |
|---|---|---|---|---|---|---|
| Gap size % of rotor chord | 10% | | 20% | | 20% | |
| Rotor-stator pitch ratio | 1.45 | | 1.45 | | 0.94 | |
| $S_r/C$ | 0.618 | | 0.618 | | 0.618 | |
| $\theta$ | 40 deg | | 40 deg | | 40 deg | |
| $M$ | 0.6 | | 0.6 | | 0.6 | |
| $\beta$ | 14.7 | | 14.7 | | 9.54 | |
| $\omega$ | 20.4 | | 21.35 | | 13.8 | |
| | Mag. | Phase | Mag. | Phase | Mag. | Phase |
| Max normalized enthalpy variation ($\rho\bar{H}/\bar{P}_{TE}$) amplitude and phase[a] from | | | | | | |
| UNSFLO | 0.175 | 14.6 deg | 0.160 | 37.3 deg | 0.264 | 56.9 deg |
| LINSUB | 0.170 | 34.9 deg | 0.158 | 42.2 deg | 0.220 | 27.4 deg |
| Difference | <0.2% | 20.3 deg | <2% | 3.9 deg | 20% | 29.5 deg |

[a]Phase of peak relative to stator leading edge.

in Cambridge.[14] The required inputs to the program are tabulated in Table A1. The direct output of the program is the vortex sheet strength shed from the rotor $\bar{\varepsilon}$. This quantity can be easily converted to the circulation on the blade by Kelvin's theorem

$$\bar{\Gamma} = -(i\bar{\varepsilon}/\omega)$$

and then to the stagnation enthalpy variation by Eq. (7). Table A2 shows the flow parameters and results from both LINSUB and UNSFLO for three cases presented earlier. The relative magnitude and phase angle difference are also included. The agreement between the two methods are excellent. Keep in mind that the possible errors related to the two methods are fundamentally different. One is numerical errors and the other is errors from the assumption of flat plate cascade and linearization. This shows that LINSUB is a reliable alternative approach to this research.

The effect of rotor stator gap can be shown, using LINSUB, in a more quantitative way. Assuming that the stator blade generates a pressure perturbation of $\bar{P}_{10}$ in magnitude at an axial position, say 10% upstream of the stator, thus from Eq. (A1)

$$\bar{P}_{TE} = \bar{P}_{10} \exp[i\alpha(\delta - 0.1)\cos\theta]$$

This pressure perturbation is only a function of the stator geometry and loading, with constant value for different gap sizes $\delta$. The factor of cos $\theta$ is because in Eq. (A1) the normalizing length scale is the true chord of the blade, not the axial chord.

If we use the pressure variation $\bar{P}_{10}$ as the normalizing quantity, then the stagnation enthalpy $\rho\bar{H}/\bar{P}_{10}$ is

$$\frac{\rho\bar{H}}{\bar{P}_{10}} = \text{const} \exp[i\alpha(\delta - 0.1)\cos\theta]$$

where the constant is independent of the gap size $\delta$. Besides a phase shift, the magnitude of $\rho\bar{H}/\bar{P}_{10}$ decays exponentially with a decay rate equal to the pressure decay rate from the stator blade row. This is shown in Fig. A2. The solid line is the exponential function while the other two sets of symbols represent the results from both UNSFLO and LINSUB calculations.

Using LINSUB to explore the effect of different pitch ratio is a little more complicated. The circumferential wave number $\beta$ and the reduced frequency $\omega$ are all functions of the pitch ratio. Specifically

$$\beta = 2\pi \frac{C}{S_r}\frac{S_r}{S_s}$$

$$w = \beta \frac{(V_w)}{W} = 2\pi \frac{C}{S_r}\frac{S_r}{S_s}\frac{(V_w)}{W}$$

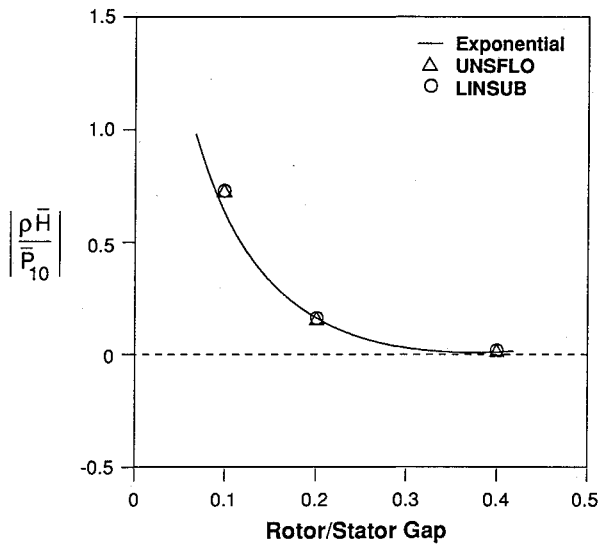


**Fig. A2 Magnitude of the normalized enthalpy fluctuation ($|\rho\bar{H}/\bar{P}_{10}|$) as a function of rotor-stator gap, showing exponential decay by UNSFLO and LINSUB.**

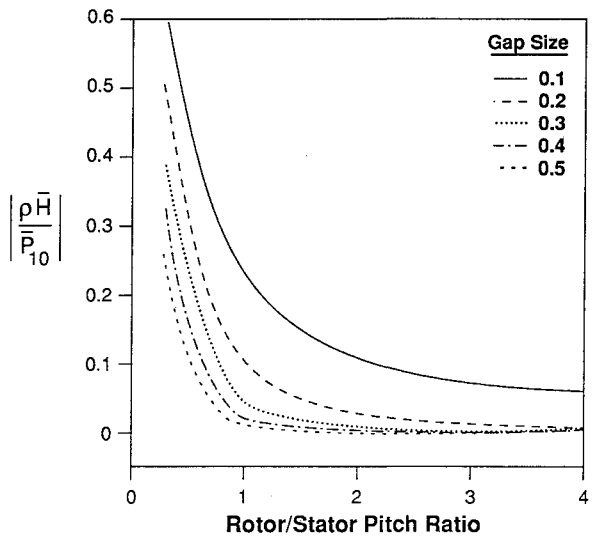


**Fig. A3 Total enthalpy variation ($|\rho\bar{H}/\bar{P}_{10}|$) as a function of pitch ratio and rotor-stator gap.**

Both of them are linear functions of pitch ratio $S_r/S_s$. The nondimensional total enthalpy variation $\rho\bar{H}/\bar{P}_{10}$ can be put in a simple functional form. Again, if we use the pressure perturbation 10% upstream of the stator, then $\rho\bar{H}/\bar{P}_{10}$ will only be a function of gap size and rotor stator pitch ratio. This relationship is shown in Fig. A3. Once again, the decrease of

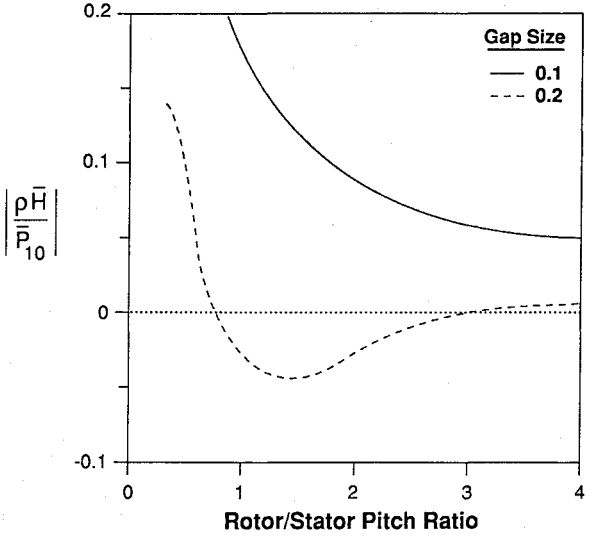


**Fig. A4 Calculated difference between probe measurement and circumferential average for different pitch ratio and rotor-stator gap.**

total enthalpy at larger gap is indicated. It also shows that $\rho\tilde{H}/\bar{P}_{10}$ decreases as pitch ratio increases. This latter trend deserves more explanation. It is true that higher pitch ratio (thus higher solidity) generates smaller pressure perturbation. But this effect is already included in the nondimensional form of $\rho\tilde{H}/\bar{P}_{10}$. In fact, the pressure decay rate shown in Eq. (A1) is proportional to pich ratio, resulting in a more uneven chordwise loading on the rotor blade. Thus, the unsteady loading on the rotor decreases as a whole.

A practical example is to project the difference between the circumferential average and a probe reading at one point, for example, the stator leading edge. Because the total enthalpy perturbations are convected along the streamline in the absolute frame, the possible probe measurement at any axial location other than the rotor trailing edge plane can be easily calculated by a simple phase shift. Take 10% upstream of the stator leading edge, for example. Since the pressure perturbation at that location can be easily calculated from any methods, including potential calculation of the stator flowfield, or panel method, only the nondimensional quantity $\rho\tilde{H}/\bar{P}_{10}$ will be presented. Without losing generality, we choose the maximum pressure point as the probe location. This point in most cases is very close to the stator leading edge. Figure A4 shows the possible difference between the probe reading and the circumferential-averaged value, for pitch ratios ranging from 0.3 to 4, and two different gap sizes of 10 and 20% of the rotor axial chord. As expected, the probe reading can well be higher or lower than the average value depending on individual situations, with the absolute value decreasing while the gap size and/or pitch ratio increases.

## Acknowledgments

The authors would like to acknowledge the active assistance of R. Haimes, as well as many useful discussions with E. M. Greitzer. M. D. Hathaway kindly provided the laser anemometry data. This work was supported by Textron Lycoming.

## References

[1]Weyer, H., "The Determination of Time-Weighted Average Pressures in Strongly Fluctuating Flows, Especially in Turbomachines," European Space Research Organization TT-161, May 1975.

[2]Cook, S. C., and Elder, R. L., "Development of a Mass Averaging Temperature Probe," AGARD CP-468, Feb. 1990.

[3]Agnew, B., Elder, R. L., and Terril, M., "An Investigation of the Response of Temperature Sensing Probes to an Unsteady Flowfield," American Society of Mechanical Engineers Paper 85-GT-223, June 1985.

[4]Pianko, M., and Wazelt, F., "Suitable Averaging Techniques in Nonuniform Internal Flows," AGARD-AR-182, June 1983.

[5]Giles, M. B., "Calculation of Unsteady Wake/Rotor Interaction," *Journal of Propulsion and Power*, Vol. 4, No. 4, 1988, pp. 356–362.

[6]Giles, M. B., "Stator/Rotor Interaction in a Transonic Turbine," AIAA Paper 88-3093, July 1988.

[7]Urasek, D. C., Gorell, W. T., and Cunnan, W. S., "Performance of Two-Stage Fan Having Low-Aspect-Ratio, First-Stage Rotor Blading," NASA TP-1493, Aug. 1979.

[8]Strazisar, A. J., and Powell, J. A., "Laser Anemometer Measurements in a Transonic Axial Flow Compressor," *Journal of Engineering for Power*, Vol. 103, No. 2, 1981, pp. 430–437.

[9]Hathaway, M. D., private communication, NASA LeRC, 1988.

[10]Gertz, J. B., "Unsteady Design-Point Flow Phenomena in Transonic Compressors," Ph.D. Dissertation, Massachusetts Inst. of Technology, Cambridge, MA, 1985.

[11]Wood, J. R., Strazisar, A. J., and Simonyi, P. S., "Shock Structure in a Transonic Fan Using Laser Anemometry," AGARD CP-401, Sept. 1986.

[12]Owen, P. R., "Computational Simulation of Unsteady Flow in an Transonic Compressor Rotor," M.S. Dissertation, Massachusetts Inst. of Technology, Cambridge, MA, 1986.

[13]Horlock, J. H., and Daneshyar, H., "Stagnation Pressure Changes in Unsteady Flow," *Aeronautical Quarterly*, Vol. XXII, Aug. 1971, pp. 207–224.

[14]Whitehead, D. S., *LINSUB User's Guide*, personal communication, Univ. of Cambridge.

[15]Smith, S. N., "Discrete Frequency Sound Generation in Axial Flow Turbomachines," Univ. of Cambridge, Dept. of Engineering Rept. CUED/A-TURBO/TR-29, 1971.